ECS Journal of Solid State Science and Technology, **3** (5) P133-P137 (2014)
2162-8769/2014/3(5)/P133/5/$31.00 © The Electrochemical Society

Ambient Degradation of ZnO Powders: Does Surface Polarity Matter?

Jiaqi Cheng and Kristin M. Poduska[*,z]

Departments of Chemistry & Physics and Physical Oceanography, Memorial University of Newfoundland, St. John's NL A1B 3X7, Canada

Comparing different synthesis methods to investigate ambient degradation differences among ZnO crystals with different crystal habits, we examined the effects of particle size, surface area, shape (surface polarity), and zeta (surface) potential. Neither surface polarity nor surface area, on their own, can account for the differences in the surface carbonation among differently synthesized ZnO samples. Our results demonstrate that surface dissolution and carbonation tendencies must be considered together, in the context of surface polarity, to explain different propensities toward degradation in ZnO powders.

Manuscript submitted February 10, 2014; revised manuscript received March 3, 2014. Published March 13, 2014.

The surface reactivity of ZnO makes this material appealing for technological applications such as UV photodetection and electrical sensors,[1,2] but it also makes it prone to instability and degradation over the long-term. This aging problem can have a strong adverse effect on the material's optical, electrical, and mechanical properties,[3,4] and it is especially pronounced in materials with high surface area.[5] Even though there is a large body of literature related to tailoring the size and morphology of ZnO toward enhanced functionality, very few studies have investigated how these factors affect the material's long term stability.

When ZnO is immersed in water, a soluble $Zn(OH)_2$ layer is formed on the particle surface *via* chemisorption or physisorption of hydroxyl.[6,7] The rate of ZnO dissolution is then controlled by equilibrium established between $Zn(OH)_{2(s)}$ and species (e.g. $Zn^{2+}{}_{(aq)}$, $Zn(OH)^{+}{}_{(aq)}$ depending on pH) in solution phase. A generally accepted trend is that particle dissolution rate increases with reduced particle size due to increasing surface area.[3] However, to our knowledge, no study has taken in account the particle shape effect on the dissolution rate.

The ambient instability of ZnO is also well-known in the context of corrosion studies on galvanized metallic zinc coatings.[8-10] The oxidation layer of ZnO that forms on a Zn metal surface can react readily with ambient CO_2, moisture, and other airborne gaseous species. It is generally accepted that Zn corrosion involves surface dissolution of ZnO due to a thin surface water layer that is acidified by dissolved atmospheric CO_2. This dissolution and carbonation sequence converts ZnO into $Zn_5(OH)_6(CO_3)_2$ (hydrozincite, abbreviated here as ZHC). This ZHC layer is electrically insulating, unlike the semiconducting behavior of its ZnO precursor.

Despite its role in metal corrosion, there are few atmospheric degradation studies of ZnO. Several recent reports focused on the stability of high-temperature-grown nanowires.[11,12] After prolonged exposure to humidity and CO_2, ZHC bunches were first observed in electron microscopy studies of thermally deposited ZnO nanowires. Subsequently, second harmonic generation spectroscopy on similarly prepared samples showed the growth patterns of ZHC forming on single ZnO nanowires.[12] There remains a lack of data on the degradation tendencies of ZnO prepared by liquid-based methods, at lower temperatures, and/or with other crystal habits, even though there are numerous reports of new synthesis methods for more economical synthesis of ZnO by using these strategies.

One factor that makes nanowires different from other shapes of ZnO crystallites is that this morphology tends to expose predominantly non-polar faces, as shown schematically in Fig. 1. Rod-shaped ZnO is regarded as the most stable shape of ZnO because of its many low energy non-polar facets.[13] In contrast, a pyramid is a non-classical shape for ZnO because all facets exposed on a ZnO pyramid are high-energy polar surfaces.

In this work, we explore the role that surface polarity can play in regulating surface carbonation in ZnO powders, since the presence of an electrically insulating carbonate can have dire consequences for using ZnO in electronic or optical device applications. Different synthesis methods facilitate our investigation of ambient degradation rates of bare ZnO crystallites with different crystal habits, examining factors including particle size, surface area, shape (surface polarity), and zeta potential. Our results demonstrate that surface dissolution and carbonation tendencies are closely linked in ZnO, while surface area and polarity alone are not necessarily the most diagnostic parameters for tracking degradation tendencies.

Experimental

Synthesis.— We utilized several distinct synthesis strategies to produce either faceted or mixed polarity (irregularly shaped) crystallites, while avoiding organic surfactants and other surface stabilizers. All reagents were analytical grade and used as received.

Predominantly polar-faceted MS-ZnO particles with pyramid shapes were prepared by a molten-salt-assisted route, adapted from methods reported by others.[14,15] In our experiments, $Zn(O_2CCH_3)_2{\cdot}2H_2O$ (Caledon) at 1 mM was mixed well with 0.1 M $LiNO_3$ (Aldrich) in an alumina crucible for ~6.5 g total mass. The mixture was heated in air at 500°C for 1 hour, then removed from the oven and cooled in air. Excess $LiNO_3$ was removed by washing and filtering the product many times with ultrapure water (Barnstead Nanopure 18.2 MΩ) until the filtrate pH approached 7.

Predominantly non-polar-terminated MA-ZnO particles were rod-like, and were prepared using a solvent-free solid-state metathesis reaction[16] followed by annealing. In powder form, NaOH (EM Science) and $ZnCl_2$ (Caledon) salts were ground together in 2:1 ratio. A self-sustained exothermic reaction that produced ZnO was triggered after about 2 minutes of grinding. The byproducts were removed by intensive washing and filtering with ultrapure water until the pH of the filtrate approached 7. The remaining product was then oven-dried at 85°C in air and then heated for 8 hrs in air at 500°C, which is well below the melting point of ZnO (2248 K).

Irregularly shaped M-ZnO particles were prepared identically to the MA-ZnO particles described above, but without the annealing step.

Smaller-sized irregularly shaped ZnO (ST-ZnO) was prepared solvothermally by refluxing 50 mM $Zn(O_2CCH_3)_2{\cdot}2H_2O$ (Caledon) with 50 mM NaOH (EM Science) in ethanol for 6 hours at 80°C, adapted from a method reported by others.[17] The resulting white precipitate was washed several times with ultrapure water and separated *via* centrifugation before oven-drying at 85°C in air.

Material characterization.— Crystalline phases and their average domain sizes were assessed by powder X-ray diffraction (PXRD; Rigaku Ultima IV X-ray diffractometer with Cu Kα at 3°/min, step size 0.02°; lattice constant refinements from Jade software (Materials Data

[*]Electrochemical Society Active Member.
[z]E-mail: kris@mun.ca

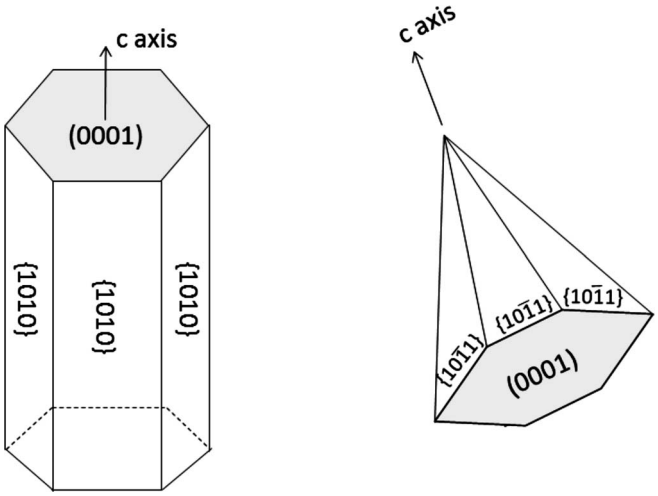

Figure 1. Schematic illustration of different polar and non-polar faces for ZnO. The conventional hexagonal rod (left) has many low energy (1010) non-polar facets exposed, while the hexagonal pyramid (right) presents polar (10$\bar{1}$1) facets. In both illustrations, the basal face is polar (0001).

Inc.) and compared with JCPDS[18] data). Particle size distributions were also measured with dynamic light scattering (DLS; Malvern Nano S Zetasizer, measurement range: 0.3 nm to 10.0 μm). Particle shapes were determined from scanning electron microscopy images (SEM, FEI Quanta 400).

Surface compositions for fresh samples were investigated with X-ray Photoelectron Spectroscopy (XPS) data collected with a VG Microtech MultiLab ESCA 2000. The surface areas of the samples were evaluated by the Brunauer-Emmet-Teller (BET) method at a relative pressure ratio of 0.1-0.35. Zeta potentials were measured in aqueous solutions: 5% v/v of freshly made ZnO samples were immersed in ultrapure water that had been prepared at either an initial pH 5 (using HCl) or initial pH 11 (using NaOH). The suspensions were sealed and then magnetically stirred for 24 hours and sonicated for 1 hour prior to measurements (Malvern Nano S Zetasizer). The aged pH values of the suspensions were also recorded. Qualitative assessments of sample dissolution were compared through the hydrodynamic diameters of particles equilibrated under acidic conditions and alkaline conditions.

Long-term atmospheric carbonation.— To investigate the long-term ambient carbonation of ZnO, 200 mg of each sample was placed in a sealed chamber (500 mL volume) with opaque walls to prevent photolysis.[4] The relative humidity (RH) inside the chamber was maintained at 93 ± 2% at 22°C with the equilibrium vapor pressure of a saturated KNO_3 solution.[19] High CO_2 concentrations were achieved by sublimating 50 mg of dry ice in the chamber. All samples were stored under high humidity and CO_2 conditions for 2 weeks prior to the degradation assessments. The degradation products were assessed with Fourier transform infrared spectroscopy (FTIR; Alpha spectrometer (Bruker, Billerica, MA, U.S.A.) at 4 cm^{-1} resolution on powdered samples dispersed in a 7 mm diameter KBr pellet). FTIR is an effective method to assess the extent of ZnO carbonation because it identifies both crystalline and poorly crystalline phases, without introducing heating effects that could alter the atmospheric carbonation product. Separate decomposition experiments with thermogravimetric analysis (TGA) were conducted with a Q500 thermogravimetric analyzer (TA Instruments, New Castle, DE, U.S.A.) using a Pt pan and heating to 600°C at 20.00°C/min under 40.0 mL/min N_2 gas flow).

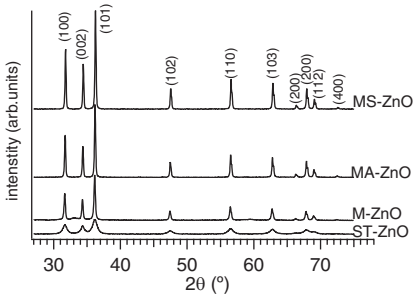

Figure 2. Representative XRD data for ZnO prepared by four different synthesis methods. In each case, all diffraction peaks can be indexed to wurtzite-type ZnO (JCPDS 36-1451).

Results and Discussion

Bulk characterization.— XRD data (Fig. 2) show that all of the different synthesis methods yield ZnO as the only crystalline product. In each case, all diffraction peaks can be indexed to wurtzite-type ZnO (JCPDS 36-1451). However, the particle sizes and morphologies are quite different among the four different products, as shown in Fig. 3 and summarized in Table I.

The molten-salt-assisted growth (MS-ZnO) produced the largest particles, exhibiting hexagonal pyramid shapes that were often twinned at the base (Fig. 3(c)). Others have suggested that the excess Li^+ present in the molten salt during crystallite growth can electrostatically passivate the polar {10$\bar{1}$1} faces to slow their growth rate, since heating in the absence of molten $LiNO_3$ yields a conventional rod shape.[15]

The metathesis-produced M-ZnO has irregular crystallite shapes (Fig. 3(a)), which is not surprising in light of its extraordinarily fast crystallization time (~1 min). Others have attributed irregular particle shapes to the lack of solvent in this solid-state method that would promote diffusion-related crystal ripening.[20] After annealing, the MA-ZnO particle size increases relative to M-ZnO, and it also transforms into a rod-like shape (Fig. 3(b)).

Solvothermal methods (ST-ZnO) produce the smallest particles (20 ± 10 nm), based on DLS data and Scherrer analyzes of XRD peak widths (Table 1). This method of refluxing zinc salts and OH^- in an alcoholic medium is one of the most commonly employed methods for making ZnO nanocrystals.[17,21-24] The lower solubility of the precursor

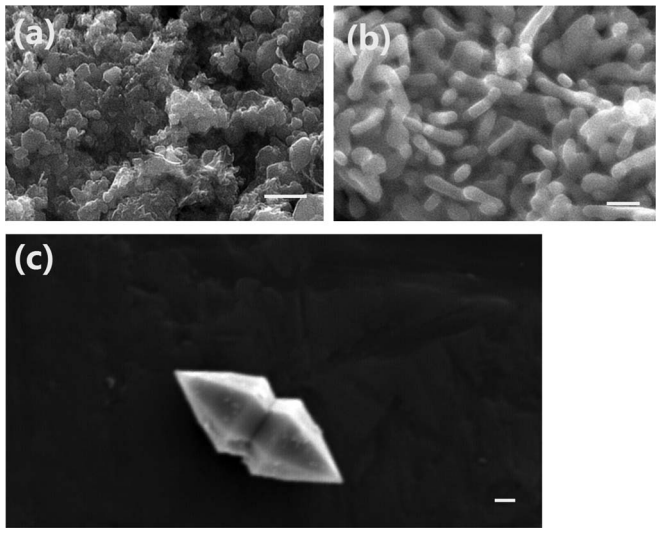

Figure 3. Representative SEM images for freshly made (a) M-ZnO (b) MA-ZnO and (c) MS-ZnO samples. In each image, the scale bar represents 200 nm.

Table I. Comparisons of ZnO sizes (from DLS data) and surface areas (from BET measurements), and changes to mean particle size after exposure to acidic solution (pH 5).

Synthesis method (abbreviation)	size (nm)	surface area (m^2g^{-1})	mean size change at pH 5 (%)
Molten-salt-assisted (MS-ZnO)	1000 ± 500	4.2 ± 0.3	–10 ± 2
Annealed metathesis (MA-ZnO)	400 ± 100	2.8 ± 0.3	–15 ± 5
Metathesis (M-ZnO)	100 ± 50	3.4 ± 0.3	–90 ± 20
Solvothermal (ST-ZnO)	20 ± 10	9.4 ± 0.3	–50 ± 10

salts (such as $ZnCl_2$ or $Zn(O_2CCH_3)_2$) in alcohol relative to aqueous media would presumably lead to both faster nucleation and slower ripening, but this has not yet been studied in detail.[13]

Surface characterization: short-term degradation.— Surface compositions of freshly made samples were investigated with XPS (Fig. 4). Gaussian fits to the O 1*s* spectra (Fig. 4(a)) yield up to three peaks: 530.7 eV corresponds to lattice O in ZnO, 533 eV is due to O from surface hydroxides (OH), and the peak at 535 eV is from O from carbonate species.[25] No evidence of carbonates was present for either MA-ZnO or ST-ZnO. The Zn $2p_{2/3}$ peak was centered on 1021.7 eV to correspond with the usual 2+ oxidation state for Zn.[26] There were slight variations in the peak width for Zn $2p_{2/3}$, with M-ZnO the largest and ZnO-MA the narrowest.

To probe surface differences in an aqueous environment, the zeta potential for each kind of ZnO preparation was measured as a function of aged pH of the suspensions (Fig. 5). There are two distinct groupings. Suspensions that started with pH 11 showed only slight increases in acidity with aging (pH ≥ 10) and had large negative zeta potentials (–40 to –60 mV). These large zeta potentials are consistent with earlier reports that have shown that ZnO displays good colloidal stability at alkaline pH values.[7] However, suspensions with an initial pH = 5 aged to considerably more alkaline values (6.5–7.5) and displayed positive zeta potentials with smaller magnitudes (+10 for most, with M-ZnO at +22 mV). The lone exception to this trend is MS-ZnO, which shows a negative zeta potential that is uncharacteristic for ZnO (whose isoelectric point ranges from 8.5 to 10.5). This anomaly is likely due to surface carbonation: XPS data (Fig. 4) shows clear evidence of this in MS-ZnO, and carbonates such as ZHC have been reported to have a negative zeta potential in this pH range.[27]

The pH shifts in aged suspensions are a results of different degrees of surface dissolution to equilibrate with the aqueous environment. A qualitative comparison of the relative dissolution tendencies emerges by comparing the mean hydrodynamic particle sizes after equilibrating in either the acidic (initial pH 5) or basic (initial pH 11) water (Table I). In all cases, the mean particle size from more alkaline suspensions is consistent with the particle sizes extracted from XRD peak widths. Also true in all cases is that the more acidic suspensions show smaller particle sizes, as expected. However, there is considerable variability in the extent of the size reduction, with the most severe dissolution occurring for M-ZnO.

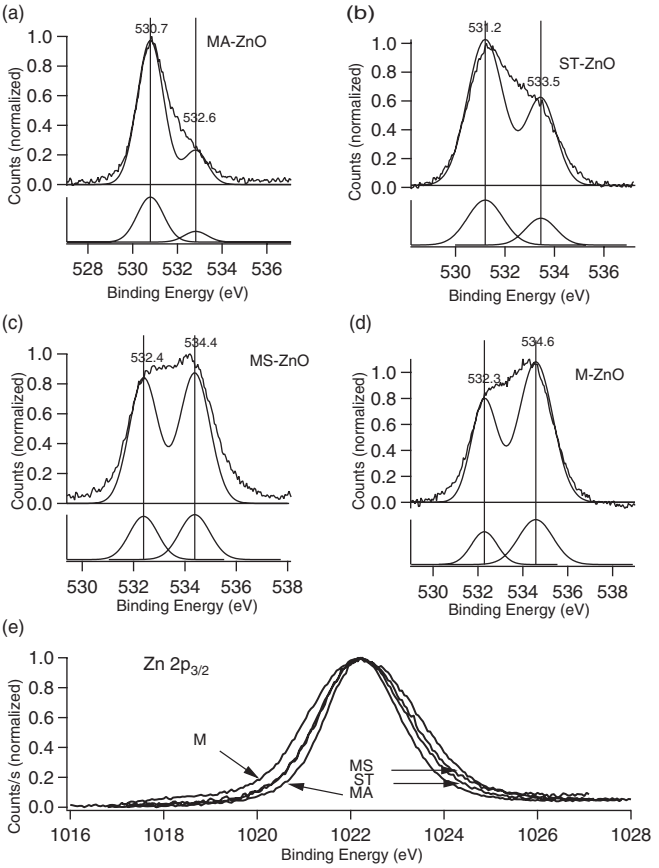

Figure 4. XPS data for (a,b,c,d) O 1*s*, and (e) Zn $2p_{2/3}$ for fresh ZnO synthesized by different methods.

Long-term atmospheric degradation.— The differences in short-term carbonation and dissolution that appear in XPS data (Fig. 4 and DLS data (Fig. 5 inset) are amplified when long-term degradation changes are monitored. Fig. 6(a) shows representative FTIR spectra for freshly made samples. With all four syntheses, only the Zn-O lattice modes (a broad peak near 450 cm^{-1}) are apparent, which is consistent with the XRD data shown in Fig. 5. In contrast, after 30 days of exposure to CO_2 and high humidity, there are many new spectral features (Fig. 6(b)). Carbonate vibration modes due to ZHC appear between 1380 and 1510 cm^{-1}, while the peak near 950 cm^{-1} has been attributed to a Zn-OH distortion.[28,29] ST-ZnO and MA-ZnO show exclusively ZnO, MS-ZnO shows moderate ZHC formation with substantial ZnO remaining, while M-ZnO shows complete conversion to ZHC. We note that the trends for higher amounts of the ZHC decomposition product in the FTIR spectra correlate well with wider Zn $2p_{2/3}$ peaks in the XPS data.

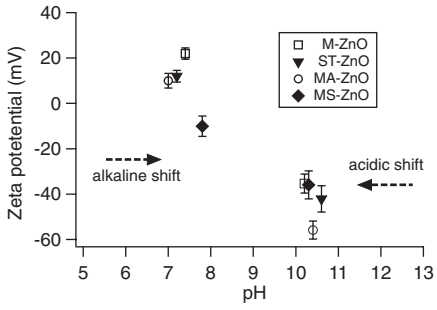

Figure 5. Zeta potentials of ZnO samples with respect to aged suspension pH. The arrows indicate the different pH shift trends for suspensions that started at pH 5 (toward more alkaline) compared to those that started at pH 11 (toward more acidic).

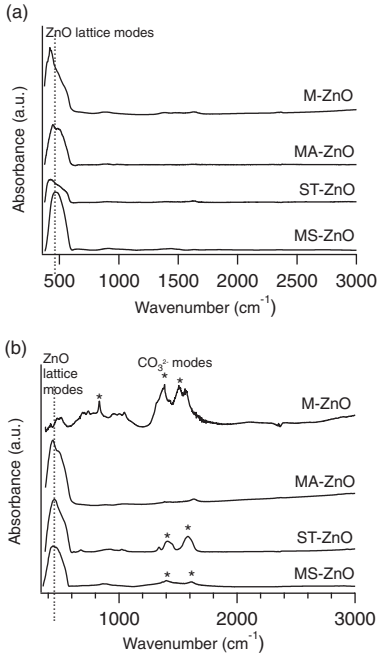

Figure 6. Representative FTIR spectra for (a) fresh samples and (b) samples aged for 30 days in a high CO_2 and high humidity environment.

To confirm the transformation from ZnO to ZHC, product from the most degradation prone preparation method (M-ZnO) was confirmed with additional FTIR measurements to monitor relative intensity changes of the Zn-O lattice mode and carbonate modes (Fig. 7(a)), and with TGA weight loss data (Fig. 7(b)). After 30 days of exposure, TGA data on the degradation product compare well with the expected theoretical weight loss of 25.5% for complete ZnO conversion to ZHC.[30]

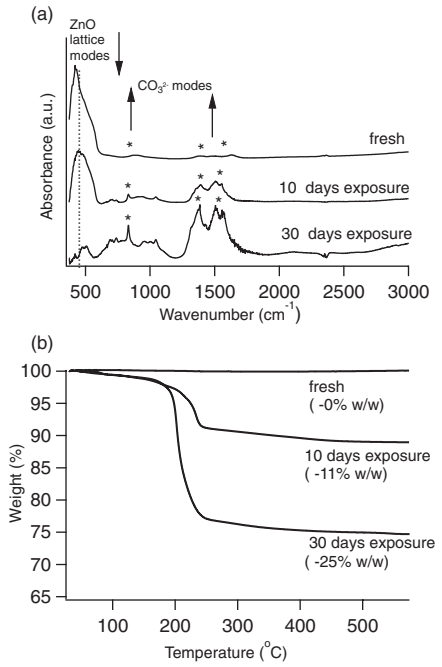

Figure 7. (a) Representative FTIR spectra of M-ZnO samples taken after exposure to high CO2 and humidity for different periods of time and (b) their corresponding TGA data. In (a), the arrows indicate that the ZnO lattice modes decrease with time, while the carbonate-related modes (denoted with an asterisk (*)) increase with time.

Discussion.— It is clear that different preparations of ZnO lead not only to distinct particle morphologies, but also to different carbonation tendencies in the ambient and when exposed to wet and CO_2-rich conditions. For reasons explained below, polar surfaces alone cannot be sufficient to explain the differences in the time evolution of the atmospheric degradation. We propose that surface dissolution, influenced by surface polarity, is a key factor that affects the extent of carbonation in these materials.

We observe that on only two of the freshly made types (M-ZnO (irregularly shaped) and MS-ZnO (polar faceted)), a thin layer of ZHC forms soon after synthesis. This layer can be detected with XPS (5-10 nm depth probe) but is not present in a large enough quantity for FTIR detection (sensitive to $\leq 1\%$ of bulk). Interestingly, it is the zeta potential measurements that highlight an important difference in the way the carbonate layer behaves on these two different ZnO preparations. On the polar MS-ZnO, the carbonate appears to be preserved under mildly acidic pH conditions, as suggested by the negative zeta potential of MS-ZnO from initially acidic aged suspensions and the small decrease in mean size. On the other hand, M-ZnO has a zeta potential consistent with pure ZnO and shows a very dramatic size decrease.

The differences in the extent of size decrease do not correlate well with original particle size, but they do match the trend in relative tendency to convert to ZHC (Fig. 6 and 7). For example, our FTIR data indicate that the ZHC layer on the irregularly shaped M-ZnO continues to grow over time at the expense of ZnO (Fig. 7(a)), while the ZHC layer on the polar MS-ZnO does not evolve as rapidly.

Based on these comparison, it seems that the carbonate layer on polar surfaces can act as a protective layer. This idea has been explored by others in the context of passivating film formation on Zn metal.[27] In general, polar surfaces are expected to have higher surface energies[31] which would be consistent with an increased tendency toward humidity-related degradation. This is in line with our XPS results for surface composition, with the least surface carbonation present on the samples with a higher proportion of non-polar (low-energy) surfaces, namely the rod-like MA-ZnO.

Some have suggested that the hydrophobic nature of ZHC can substantially retard the rate of further ZnO carbonation.[32] However, more recent studies on thermally produced ZnO nanowires concluded that the formation of a ZHC layer inhibits ZnO attack initially, but degradation of the ZnO core is not completely suppressed because the ZHC film is less compact than the underlying ZnO.[11,12] These observation by others, along with the suppressed degradation we see after annealing our ZnO, suggests that the persistent atmospheric degradation of M-ZnO is likely due to a higher concentration of defects (plausibly due to its fast crystallization process) that make the particle surface more prone to humidity-assisted dissolution.[30]

It is worthy of note that the extent of the carbonation differences shown in Figs. 5 and 6 do not correlate directly with surface area. For example, the most reactive samples are M-ZnO (BET surface area 3.6 m^2g^{-1}), while the synthesis method that produces the highest surface area product (ST-ZnO, with BET surface area of 9.4 m^2g^{-1}) shows the least evidence of carbonation. Taken together, our analyzes show that other factors related to the surface composition have a larger effect on the relative tendency of ZnO toward atmospheric carbonation.

Conclusions

Surface polarity impacts the carbonation rates among the differently synthesized ZnO samples, but it is not necessarily the dominant factor. In particular, ZnO produced in rapid reactions can be more susceptible to ambient carbonation; we demonstrate an extreme case wherein exposure to high ambient humidity and CO_2 levels leads to complete conversion of ZnO to $Zn_5(OH)_6(CO_3)_2$ in less than one month. This transformation from a semiconducting metal oxide material to an insulating carbonate phase would have profound impacts on the electrical and optical properties of the product, and could have devastating effects in device applications. While others have

have shown that ZnO nanowire degradation can be mitigated by applying a protective coating of compact alumina or titania using atomic layer deposition,[4,11,12] our work shows that synthesis and annealing conditions alone can have a dramatic effect on the tendency for ZnO powders to degrade in ambient environments.

Extending beyond the specific case of ZnO, these results are generally important for metathesis reactions and other rapid syntheses for producing nanocrystalline materials.[16,20,30,33-37] Since nanostructured materials made by solid-state metathesis have been utilized for solar cell,[35] cathode material,[38] UV-detector[36] and gas sensor[34,39,40] applications, it is important to recognize the tradeoffs between rapid production and long-term stability against atmospheric degradation.

Acknowledgments

Natural Science and Engineering Resource Council (Canada), Petroleum Research Atlantic Canada, and the Canada Foundation for Innovation (New Opportunities) funded this work. K. Kenneally, J. Wells, and H. Hirasawa assisted with sample preparation. W. Aylward (PXRD), J. Collins (TGA), and M. Shaffer (SEM) granted use of the facilities they manage through Memorial University Core Research Equipment and Instrument Training network. V. Booth at Memorial University granted use of DLS and zeta potential instrumentation. J. Wen and A. Chen conducted the BET measurements at Lakehead University, Thunder Bay, Ontario, Canada. Z. Bayindir conducted the XPS measurements at the Dalhousie University Facilities for Materials Characterization managed by the Institute for Research in Materials, which is funded by the Atlantic Innovation Fund and other partners.

References

1. C. Soci, A. Zhang, B. Xiang, S. A. Dayeh, D. P. R. Aplin, J. Park, X. Y. Bao, Y. H. Lo, and D. Wang, *Nano Lett.*, **7**, 1003 (2007).
2. J. Zhang, S. Wang, M. Xu, Y. Wang, B. Zhu, S. Zhang, W. Huang, and S. Wu, *Cryst. Growth Des.*, **9**, 3532 (2009).
3. I. A. Mudunkotuwa, T. Rupasinghe, C.-M. Wu, and V. H. Grassian, *Langmuir*, **28**, 396 (2012).
4. Y. Yang, D. S. Kim, Y. Qin, A. Berger, R. Scholz, H. Kim, M. Knez, and U. Gosele, *J. Am. Chem. Soc.*, **131**, 13920 (2009).
5. G. V. Lowry, K. B. Gregory, S. C. Apte, and J. R. Lead, *Environ. Sci. Technol.*, **46**, 6893 (2012).
6. R. A. Reichle, K. G. McCurdy, and L. G. Hepler, *Can. J. Chem.*, **53**, 3841 (1975).
7. A. Degen and M. Kosec, *J. Eur. Ceram. Soc.*, **20**, 667 (2000).
8. T. Falk, J. Svensson, and L. Johansson, *J. Electrochem. Soc.*, **145**, 39 (1998).
9. R. Lindström, J.-E. Svensson, and L. G. Johansson, *J. Electrochem. Soc.*, **149**, B57 (2002).
10. J. Hedberg, S. Baldelli, and C. Leygraf, *J. Phys. Chem. Lett.*, **1**, 1679 (2010).
11. Z. Pan, J. Tao, Y. Zhu, J.-F. Huang, and M. P. Paranthaman, *Chem. Mater.*, **22**, 149 (2010).
12. K. A. Cimatu, S. M. Mahurin, K. A. Meyer, and R. Shaw, *J. Phys. Chem. C*, **116**, 10405 (2012).
13. B. Ludi and M. Niederberger, *Dalton Trans.*, **42**, 12554 (2013).
14. Z.-Y. Jiang, T. Xu, Z.-X. Xie, Z.-W. Lin, X. Zhou, X. Xu, R.-B. Huang, and L.-S. Zheng, *J. Phys. Chem. B*, **109**, 23269 (2005).
15. T. Xu, X. Zhou, Z. Jiang, Q. Kuang, Z. Xie, and L. Zheng, *Cryst. Growth Des.*, **9**, 192 (2009).
16. J. Cheng, M. A. Rasheed, and K. M. Poduska, *ECS J. Solid State Sci. Technol.*, **2**, Q23 (2013).
17. J. Gupta, K. Barick, and D. Bahadur, *J. Alloys Compd.*, **509**, 6725 (2011).
18. Powder Diffraction File "Joint Commission on Powder Diffraction Standards – International Centre for Diffraction Data", 2003.
19. L. B. Rockland, *Anal. Chem.*, **32**, 1375 (1960).
20. X. R. Ye, D. Z. Jia, J. Q. Yu, X. Q. Xin, and Z. Xue, *Adv. Mater.*, **11**, 941 (1999).
21. Z. Hu, G. Oskam, and P. C. Searson, *J. Colloid Interface Sci.*, **263**, 454 (2003).
22. Z. Hu, G. Oskam, R. L. Penn, N. Pesika, and P. C. Searson, *J. Phys. Chem. B*, **107**, 3124 (2003).
23. Z. Hu, J. F. H. Santos, G. Oskam, and P. C. Searson, *J.Colloid Interface Sci.*, **288**, 313 (2005).
24. A. G. Vega-Poot, G. Rodriguez-Gattorno, O. E. Soberanis-Dominguez, R. T. Patino-Diaz, M. Espinosa-Pesqueira, and G. Oskam, *Nanoscale*, **2**, 2710 (2010).
25. R. Al-Gaashani, S. Radiman, A. Daud, N. Tabet, and Y. Al-Douri, *Ceram. Inter.*, **39**, 2283 (2013).
26. J. Zheng, Q. Jiang, and J. Lian, *App. Sur. Sci.*, **257**, 5083 (2011).
27. T. H. Muster and I. S. Cole, *Corr. Sci.*, **46**, 2319 (2004).
28. M. C. Hales and R. L. Frost, *Polyhedron*, **26**, 4955 (2007).
29. B. Su, M. Li, Z. Shi, and Q. Lu, *Langmuir*, **25**, 3640 (2009).
30. J. Cheng and K. M. Poduska, *Nanomater.*, **3**, 317 (2013).
31. J. Goniakowski, F. Finocchi, and C. Noguera, *Rep. Prog. Phys.*, **71**, 016501 (2008).
32. Y. Hamlaoui, F. Pedraza, and L. Tifouti, *Corr. Sci.*, **50**, 1558 (2008).
33. L. Ren, Q. Wu, C. Yang, L. Zhu, C. Li, P. Zhang, H. Zhang, X. Meng, and F.-S. Xiao, *J. Am. Chem. Soc.*, **134**, 15173 (2012).
34. Y. Cao, D. Jia, R. Wang, and J. Luo, *Solid-State Electronics*, **82**, 67 (2013).
35. Y. Shi, K. Wang, Y. Du, H. Zhang, J. Gu, C. Zhu, L. Wang, W. Guo, A. Hagfeldt, N. Wang, and T. Ma, *Adv. Mater.*, 4413 (2013).
36. S. Mishra, R. Srivastava, and S. Prakash, *J. Mater. Sci.: Mater. Electron.*, **24**, 125 (2013).
37. R. Wang, D. Jia, and Y. Cao, *Electrochimica Acta*, **72**, 101 (2012).
38. R. Jiang, Y. Huang, D. Jia, L. Wang, and L. Wang, *J. Electrochemical Soc.*, **154**, A698 (2007).
39. Y. Cao, P. Hu, W. Pan, Y. Huang, and D. Jia, *Sens. Actuators B*, **134**, 462 (2008).
40. Z.-P. Sun, L. Liu, L. Zhang, and D.-Z. Jia, *Nanotechnology*, **17**, 2266 (2006).